Please note that terminology in this background text is different than the terminology that I teach. The underlying concepts are the same and my terminology unifies things better. Alas, my textbook is not yet written.

Chapter 3

Image processing

Figure 3.1 Some common image processing operations: (a) original image; (b) increased contrast; (c) change in hue; (d) "posterized" (quantized colors); (e) blurred; (f) rotated.

Now that we have seen how images are formed through the interaction of 3D scene elements, lighting, and camera optics and sensors, let us look at the first stage in most computer vision applications, namely the use of image processing to preprocess the image and convert it into a form suitable for further analysis. Examples of such operations include exposure correction and color balancing, the reduction of image noise, increasing sharpness, or straightening the image by rotating it (Figure 3.1). While some may consider image processing to be outside the purview of computer vision, most computer vision applications, such as computational photography and even recognition, require care in designing the image processing stages in order to achieve acceptable results.

In this chapter, we review standard image processing operators that map pixel values from one image to another. Image processing is often taught in electrical engineering departments as a follow-on course to an introductory course in signal processing (Oppenheim and Schafer 1996; Oppenheim, Schafer, and Buck 1999). There are several popular textbooks for image processing (Crane 1997; Gomes and Velho 1997; Jähne 1997; Pratt 2007; Russ 2007; Burger and Burge 2008; Gonzales and Woods 2008).

We begin this chapter with the simplest kind of image transforms, namely those that manipulate each pixel independently of its neighbors (Section 3.1). Such transforms are often called *point operators* or *point processes*. Next, we examine *neighborhood* (area-based) operators, where each new pixel's value depends on a small number of neighboring input values (Sections 3.2 and 3.3). A convenient tool to analyze (and sometimes accelerate) such neighborhood operations is the *Fourier Transform*, which we cover in Section 3.4. Neighborhood operators can be cascaded to form *image pyramids* and *wavelets*, which are useful for analyzing images at a variety of resolutions (scales) and for accelerating certain operations (Section 3.5). Another important class of global operators are *geometric transformations*, such as rotations, shears, and perspective deformations (Section 3.6). Finally, we introduce *global optimization* approaches to image processing, which involve the minimization of an energy functional or, equivalently, optimal estimation using Bayesian *Markov random field* models (Section 3.7).

3.1 Point operators

The simplest kinds of image processing transforms are *point operators*, where each output pixel's value depends on only the corresponding input pixel value (plus, potentially, some globally collected information or parameters). Examples of such operators include brightness and contrast adjustments (Figure 3.2) as well as color correction and transformations. In the image processing literature, such operations are also known as *point processes* (Crane 1997).

We begin this section with a quick review of simple point operators such as brightness

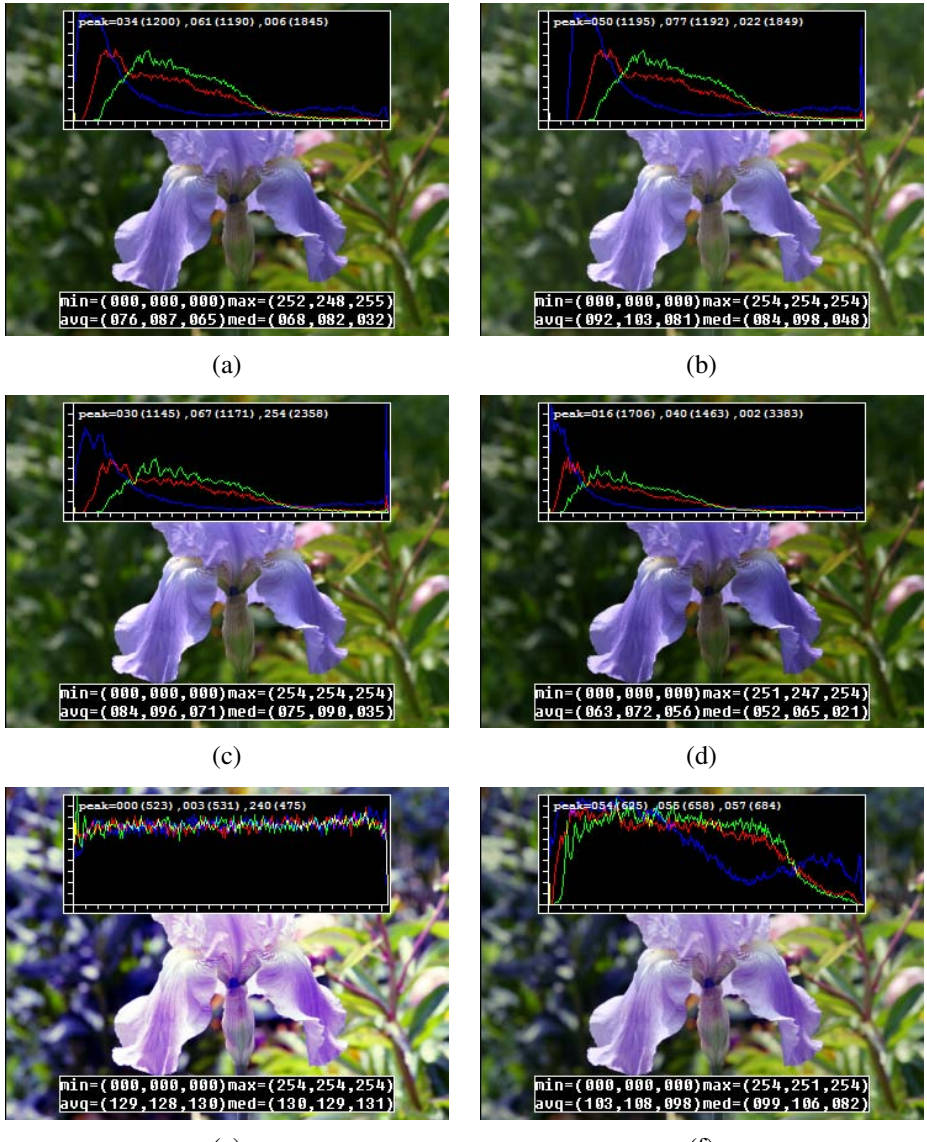

Figure 3.2 Some local image processing operations: (a) original image along with its three color (per-channel) histograms; (b) brightness increased (additive offset, $b = 16$); (c) contrast increased (multiplicative gain, $a = 1.1$); (d) gamma (partially) linearized ($\gamma = 1.2$); (e) full histogram equalization; (f) partial histogram equalization.

(a)

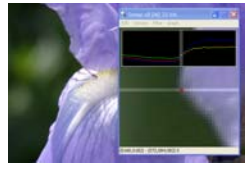

(b)

45	60	98	127	132	133	137	133
46	65	98	123	126	128	131	133
47	65	96	115	119	123	135	137
47	63	91	107	113	122	138	134
50	59	80	97	110	123	133	134
49	53	68	83	97	113	128	133
50	50	58	70	84	102	116	126
50	50	52	58	69	86	101	120

(c)

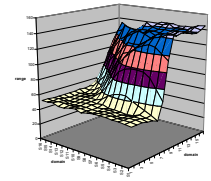

(d)

Figure 3.3 Visualizing image data: (a) original image; (b) cropped portion and scanline plot using an image inspection tool; (c) grid of numbers; (d) surface plot. For figures (c)–(d), the image was first converted to grayscale.

scaling and image addition. Next, we discuss how colors in images can be manipulated. We then present *image compositing* and *matting* operations, which play an important role in computational photography (Chapter 10) and computer graphics applications. Finally, we describe the more global process of *histogram equalization*. We close with an example application that manipulates *tonal values* (exposure and contrast) to improve image appearance.

3.1.1 Pixel transforms

A general image processing *operator* is a function that takes one or more input images and produces an output image. In the continuous domain, this can be denoted as

$$g(\boldsymbol{x}) = h(f(\boldsymbol{x})) \;\text{ or }\; g(\boldsymbol{x}) = h(f_0(\boldsymbol{x}), \ldots, f_n(\boldsymbol{x})), \tag{3.1}$$

where $\boldsymbol{x}$ is in the D-dimensional *domain* of the functions (usually $D = 2$ for images) and the functions f and g operate over some *range*, which can either be scalar or vector-valued, e.g., for color images or 2D motion. For discrete (sampled) images, the domain consists of a finite number of *pixel locations*, $\boldsymbol{x} = (i, j)$, and we can write

$$g(i, j) = h(f(i, j)). \tag{3.2}$$

Figure 3.3 shows how an image can be represented either by its color (appearance), as a grid of numbers, or as a two-dimensional function (surface plot).

Two commonly used point processes are multiplication and addition with a constant,

$$g(\boldsymbol{x}) = af(\boldsymbol{x}) + b. \tag{3.3}$$

The parameters $a > 0$ and b are often called the *gain* and *bias* parameters; sometimes these parameters are said to control *contrast* and *brightness*, respectively (Figures 3.2b–c).[1] The

[1] An image's luminance characteristics can also be summarized by its *key* (average luminanance) and *range* (Kopf, Uyttendaele, Deussen *et al.* 2007).

bias and gain parameters can also be spatially varying,

$$g(\boldsymbol{x}) = a(\boldsymbol{x})f(\boldsymbol{x}) + b(\boldsymbol{x}), \tag{3.4}$$

e.g., when simulating the *graded density filter* used by photographers to selectively darken the sky or when modeling vignetting in an optical system.

Multiplicative gain (both global and spatially varying) is a *linear* operation, since it obeys the *superposition principle*,

$$h(f_0 + f_1) = h(f_0) + h(f_1). \tag{3.5}$$

(We will have more to say about linear shift invariant operators in Section 3.2.) Operators such as image squaring (which is often used to get a local estimate of the *energy* in a band-pass filtered signal, see Section 3.5) are not linear.

Another commonly used *dyadic* (two-input) operator is the *linear blend* operator,

$$g(\boldsymbol{x}) = (1 - \alpha)f_0(\boldsymbol{x}) + \alpha f_1(\boldsymbol{x}). \tag{3.6}$$

By varying α from $0 \rightarrow 1$, this operator can be used to perform a temporal *cross-dissolve* between two images or videos, as seen in slide shows and film production, or as a component of image *morphing* algorithms (Section 3.6.3).

One highly used non-linear transform that is often applied to images before further processing is *gamma correction*, which is used to remove the non-linear mapping between input radiance and quantized pixel values (Section 2.3.2). To invert the gamma mapping applied by the sensor, we can use

$$g(\boldsymbol{x}) = [f(\boldsymbol{x})]^{1/\gamma}, \tag{3.7}$$

where a gamma value of $\gamma \approx 2.2$ is a reasonable fit for most digital cameras.

3.1.2 Color transforms

While color images can be treated as arbitrary vector-valued functions or collections of independent bands, it usually makes sense to think about them as highly correlated signals with strong connections to the image formation process (Section 2.2), sensor design (Section 2.3), and human perception (Section 2.3.2). Consider, for example, brightening a picture by adding a constant value to all three channels, as shown in Figure 3.2b. Can you tell if this achieves the desired effect of making the image look brighter? Can you see any undesirable side-effects or artifacts?

In fact, adding the same value to each color channel not only increases the apparent *intensity* of each pixel, it can also affect the pixel's *hue* and *saturation*. How can we define and manipulate such quantities in order to achieve the desired perceptual effects?

(a) (b) (c) (d)

Figure 3.4 Image matting and compositing (Chuang, Curless, Salesin *et al.* 2001) © 2001 IEEE: (a) source image; (b) extracted foreground object F; (c) alpha matte α shown in grayscale; (d) new composite C.

As discussed in Section 2.3.2, chromaticity coordinates (2.104) or even simpler color ratios (2.116) can first be computed and then used after manipulating (e.g., brightening) the luminance Y to re-compute a valid RGB image with the same hue and saturation. Figure 2.32g–i shows some color ratio images multiplied by the middle gray value for better visualization.

Similarly, color balancing (e.g., to compensate for incandescent lighting) can be performed either by multiplying each channel with a different scale factor or by the more complex process of mapping to XYZ color space, changing the nominal white point, and mapping back to RGB, which can be written down using a linear 3×3 *color twist* transform matrix. Exercises 2.9 and 3.1 have you explore some of these issues.

Another fun project, best attempted after you have mastered the rest of the material in this chapter, is to take a picture with a rainbow in it and enhance the strength of the rainbow (Exercise 3.29).

3.1.3 Compositing and matting

In many photo editing and visual effects applications, it is often desirable to cut a *foreground* object out of one scene and put it on top of a different *background* (Figure 3.4). The process of extracting the object from the original image is often called *matting* (Smith and Blinn 1996), while the process of inserting it into another image (without visible artifacts) is called *compositing* (Porter and Duff 1984; Blinn 1994a).

The intermediate representation used for the foreground object between these two stages is called an *alpha-matted color image* (Figure 3.4b–c). In addition to the three color RGB channels, an alpha-matted image contains a fourth *alpha* channel α (or A) that describes the relative amount of *opacity* or *fractional coverage* at each pixel (Figures 3.4c and 3.5b). The opacity is the opposite of the *transparency*. Pixels within the object are fully opaque ($\alpha = 1$), while pixels fully outside the object are transparent ($\alpha = 0$). Pixels on the boundary of the object vary smoothly between these two extremes, which hides the perceptual visible *jaggies*

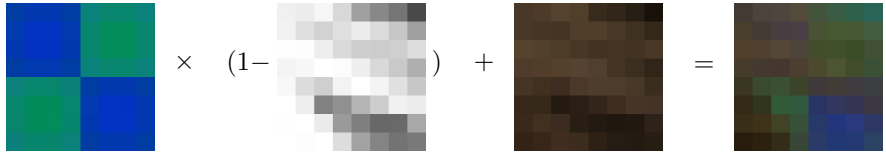

Figure 3.5 Compositing equation $C = (1 - \alpha)B + \alpha F$. The images are taken from a close-up of the region of the hair in the upper right part of the lion in Figure 3.4.

that occur if only binary opacities are used.

To composite a new (or foreground) image on top of an old (background) image, the *over operator*, first proposed by Porter and Duff (1984) and then studied extensively by Blinn (1994a; 1994b), is used,

$$C = (1 - \alpha)B + \alpha F. \tag{3.8}$$

This operator *attenuates* the influence of the background image B by a factor $(1 - \alpha)$ and then adds in the color (and opacity) values corresponding to the foreground layer F, as shown in Figure 3.5.

In many situations, it is convenient to represent the foreground colors in *pre-multiplied* form, i.e., to store (and manipulate) the αF values directly. As Blinn (1994b) shows, the pre-multiplied RGBA representation is preferred for several reasons, including the ability to blur or resample (e.g., rotate) alpha-matted images without any additional complications (just treating each RGBA band independently). However, when matting using local color consistency (Ruzon and Tomasi 2000; Chuang, Curless, Salesin *et al.* 2001), the pure unmultiplied foreground colors F are used, since these remain constant (or vary slowly) in the vicinity of the object edge.

The over operation is not the only kind of compositing operation that can be used. Porter and Duff (1984) describe a number of additional operations that can be useful in photo editing and visual effects applications. In this book, we concern ourselves with only one additional, commonly occurring case (but see Exercise 3.2).

When light reflects off clean transparent glass, the light passing through the glass and the light reflecting off the glass are simply added together (Figure 3.6). This model is useful in the analysis of *transparent motion* (Black and Anandan 1996; Szeliski, Avidan, and Anandan 2000), which occurs when such scenes are observed from a moving camera (see Section 8.5.2).

The actual process of *matting*, i.e., recovering the foreground, background, and alpha matte values from one or more images, has a rich history, which we study in Section 10.4.

Figure 3.6 An example of light reflecting off the transparent glass of a picture frame (Black and Anandan 1996) © 1996 Elsevier. You can clearly see the woman's portrait inside the picture frame superimposed with the reflection of a man's face off the glass.

Smith and Blinn (1996) have a nice survey of traditional *blue-screen matting* techniques, while Toyama, Krumm, Brumitt *et al.* (1999) review *difference matting*. More recently, there has been a lot of activity in computational photography relating to *natural image matting* (Ruzon and Tomasi 2000; Chuang, Curless, Salesin *et al.* 2001; Wang and Cohen 2007a), which attempts to extract the mattes from a single natural image (Figure 3.4a) or from extended video sequences (Chuang, Agarwala, Curless *et al.* 2002). All of these techniques are described in more detail in Section 10.4.

3.1.4 Histogram equalization

While the brightness and gain controls described in Section 3.1.1 can improve the appearance of an image, how can we automatically determine their best values? One approach might be to look at the darkest and brightest pixel values in an image and map them to pure black and pure white. Another approach might be to find the *average* value in the image, push it towards middle gray, and expand the *range* so that it more closely fills the displayable values (Kopf, Uyttendaele, Deussen *et al.* 2007).

How can we visualize the set of lightness values in an image in order to test some of these heuristics? The answer is to plot the *histogram* of the individual color channels and luminance values, as shown in Figure 3.7b.[2] From this distribution, we can compute relevant statistics such as the minimum, maximum, and average intensity values. Notice that the image in Figure 3.7a has both an excess of dark values and light values, but that the mid-range values are largely under-populated. Would it not be better if we could simultaneously brighten some

[2] The histogram is simply the *count* of the number of pixels at each gray level value. For an eight-bit image, an accumulation table with 256 entries is needed. For higher bit depths, a table with the appropriate number of entries (probably fewer than the full number of gray levels) should be used.

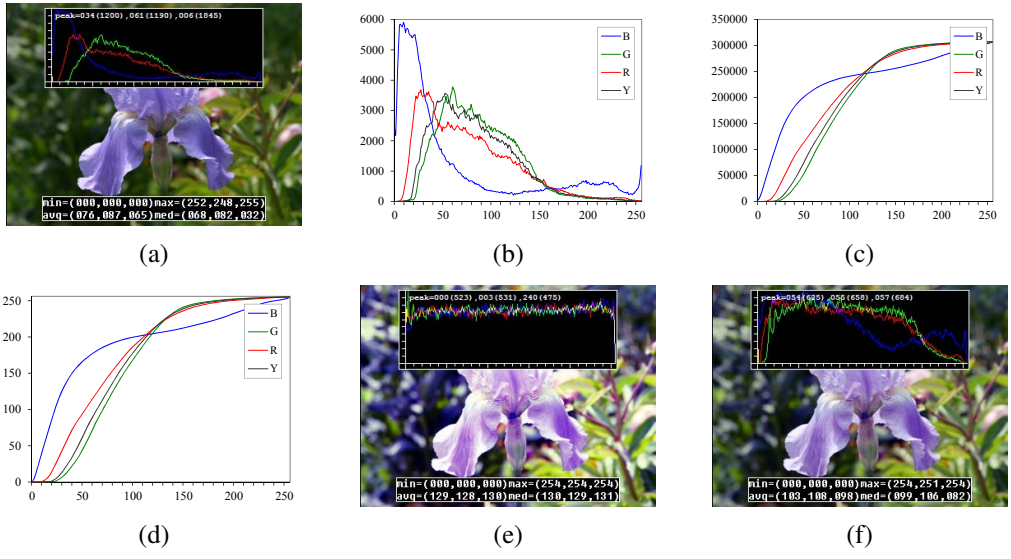

Figure 3.7 Histogram analysis and equalization: (a) original image (b) color channel and intensity (luminance) histograms; (c) cumulative distribution functions; (d) equalization (transfer) functions; (e) full histogram equalization; (f) partial histogram equalization.

dark values and darken some light values, while still using the full extent of the available dynamic range? Can you think of a mapping that might do this?

One popular answer to this question is to perform *histogram equalization*, i.e., to find an intensity mapping function $f(I)$ such that the resulting histogram is flat. The trick to finding such a mapping is the same one that people use to generate random samples from a *probability density function*, which is to first compute the *cumulative distribution function* shown in Figure 3.7c.

Think of the original histogram $h(I)$ as the distribution of grades in a class after some exam. How can we map a particular grade to its corresponding *percentile*, so that students at the 75% percentile range scored better than $^3/_4$ of their classmates? The answer is to integrate the distribution $h(I)$ to obtain the cumulative distribution $c(I)$,

$$c(I) = \frac{1}{N}\sum_{i=0}^{I} h(i) = c(I-1) + \frac{1}{N}h(I), \tag{3.9}$$

where N is the number of pixels in the image or students in the class. For any given grade or intensity, we can look up its corresponding percentile $c(I)$ and determine the final value that pixel should take. When working with eight-bit pixel values, the I and c axes are rescaled from $[0, 255]$.

(a) (b) (c)

Figure 3.8 Locally adaptive histogram equalization: (a) original image; (b) block histogram equalization; (c) full locally adaptive equalization.

Figure 3.7d shows the result of applying $f(I) = c(I)$ to the original image. As we can see, the resulting histogram is flat; so is the resulting image (it is "flat" in the sense of a lack of contrast and being muddy looking). One way to compensate for this is to only *partially* compensate for the histogram unevenness, e.g., by using a mapping function $f(I) = \alpha c(I) + (1 - \alpha)I$, which is a linear blend between the cumulative distribution function and the identity transform (a straight line). As you can see in Figure 3.7e, the resulting image maintains more of its original grayscale distribution while having a more appealing balance.

Another potential problem with histogram equalization (or, in general, image brightening) is that noise in dark regions can be amplified and become more visible. Exercise 3.6 suggests some possible ways to mitigate this, as well as alternative techniques to maintain contrast and "punch" in the original images (Larson, Rushmeier, and Piatko 1997; Stark 2000).

Locally adaptive histogram equalization

While global histogram equalization can be useful, for some images it might be preferable to apply different kinds of equalization in different regions. Consider for example the image in Figure 3.8a, which has a wide range of luminance values. Instead of computing a single curve, what if we were to subdivide the image into $M \times M$ pixel blocks and perform separate histogram equalization in each sub-block? As you can see in Figure 3.8b, the resulting image exhibits a lot of blocking artifacts, i.e., intensity discontinuities at block boundaries.

One way to eliminate blocking artifacts is to use a *moving window*, i.e., to recompute the histogram for every $M \times M$ block centered at each pixel. This process can be quite slow (M^2 operations per pixel), although with clever programming only the histogram entries corresponding to the pixels entering and leaving the block (in a raster scan across the image) need to be updated (M operations per pixel). Note that this operation is an example of the *non-linear neighborhood operations* we study in more detail in Section 3.3.1.

A more efficient approach is to compute non-overlapped block-based equalization functions as before, but to then smoothly interpolate the transfer functions as we move between

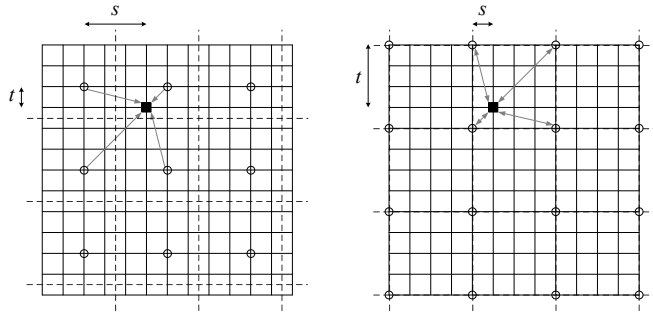

Figure 3.9 Local histogram interpolation using relative (s, t) coordinates: (a) block-based histograms, with block centers shown as circles; (b) corner-based "spline" histograms. Pixels are located on grid intersections. The black square pixel's transfer function is interpolated from the four adjacent lookup tables (gray arrows) using the computed (s, t) values. Block boundaries are shown as dashed lines.

blocks. This technique is known as *adaptive histogram equalization* (AHE) and its contrast-limited (gain-limited) version is known as CLAHE (Pizer, Amburn, Austin *et al.* 1987).[3] The weighting function for a given pixel (i, j) can be computed as a function of its horizontal and vertical position (s, t) within a block, as shown in Figure 3.9a. To blend the four lookup functions $\{f_{00}, \ldots, f_{11}\}$, a *bilinear* blending function,

$$f_{s,t}(I) = (1-s)(1-t)f_{00}(I) + s(1-t)f_{10}(I) + (1-s)tf_{01}(I) + stf_{11}(I) \quad (3.10)$$

can be used. (See Section 3.5.2 for higher-order generalizations of such *spline* functions.) Note that instead of blending the four lookup tables for each output pixel (which would be quite slow), we can instead blend the results of mapping a given pixel through the four neighboring lookups.

A variant on this algorithm is to place the lookup tables at the *corners* of each $M \times M$ block (see Figure 3.9b and Exercise 3.7). In addition to blending four lookups to compute the final value, we can also *distribute* each input pixel into four adjacent lookup tables during the histogram accumulation phase (notice that the gray arrows in Figure 3.9b point both ways), i.e.,

$$h_{k,l}(I(i, j)) \mathrel{+}= w(i, j, k, l), \quad (3.11)$$

where $w(i, j, k, l)$ is the bilinear weighting function between pixel (i, j) and lookup table (k, l). This is an example of *soft histogramming*, which is used in a variety of other applica-

[3] This algorithm is implemented in the MATLAB `adapthist` function.

tions, including the construction of SIFT feature descriptors (Section 4.1.3) and vocabulary trees (Section 14.3.2).

3.1.5 *Application*: Tonal adjustment

One of the most widely used applications of point-wise image processing operators is the manipulation of contrast or *tone* in photographs, to make them look either more attractive or more interpretable. You can get a good sense of the range of operations possible by opening up any photo manipulation tool and trying out a variety of contrast, brightness, and color manipulation options, as shown in Figures 3.2 and 3.7.

Exercises 3.1, 3.5, and 3.6 have you implement some of these operations, in order to become familiar with basic image processing operators. More sophisticated techniques for tonal adjustment (Reinhard, Ward, Pattanaik *et al.* 2005; Bae, Paris, and Durand 2006) are described in the section on high dynamic range tone mapping (Section 10.2.1).

3.2 Linear filtering

Locally adaptive histogram equalization is an example of a *neighborhood operator* or *local operator*, which uses a collection of pixel values in the vicinity of a given pixel to determine its final output value (Figure 3.10). In addition to performing local tone adjustment, neighborhood operators can be used to *filter* images in order to add soft blur, sharpen details, accentuate edges, or remove noise (Figure 3.11b–d). In this section, we look at *linear* filtering operators, which involve weighted combinations of pixels in small neighborhoods. In Section 3.3, we look at non-linear operators such as morphological filters and distance transforms.

The most commonly used type of neighborhood operator is a *linear filter*, in which an output pixel's value is determined as a weighted sum of input pixel values (Figure 3.10),

$$g(i,j) = \sum_{k,l} f(i+k, j+l)h(k,l). \tag{3.12}$$

The entries in the weight *kernel* or *mask* $h(k,l)$ are often called the *filter coefficients*. The above *correlation* operator can be more compactly notated as

$$g = f \otimes h. \tag{3.13}$$

A common variant on this formula is

$$g(i,j) = \sum_{k,l} f(i-k, j-l)h(k,l) = \sum_{k,l} f(k,l)h(i-k, j-l), \tag{3.14}$$

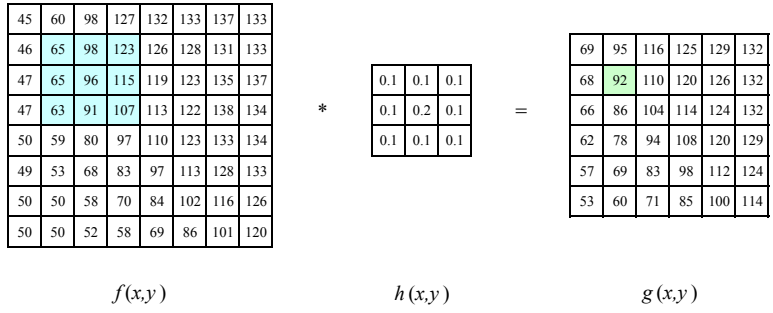

Figure 3.10 Neighborhood filtering (convolution): The image on the left is convolved with the filter in the middle to yield the image on the right. The light blue pixels indicate the source neighborhood for the light green destination pixel.

where the sign of the offsets in f has been reversed. This is called the *convolution* operator,

$$g = f * h, \tag{3.15}$$

and h is then called the *impulse response function*.[4] The reason for this name is that the kernel function, h, convolved with an impulse signal, $\delta(i, j)$ (an image that is 0 everywhere except at the origin) reproduces itself, $h * \delta = h$, whereas correlation produces the reflected signal. (Try this yourself to verify that it is so.)

In fact, Equation (3.14) can be interpreted as the superposition (addition) of shifted impulse response functions $h(i-k, j-l)$ multiplied by the input pixel values $f(k, l)$. Convolution has additional nice properties, e.g., it is both commutative and associative. As well, the Fourier transform of two convolved images is the product of their individual Fourier transforms (Section 3.4).

Both correlation and convolution are *linear shift-invariant* (LSI) operators, which obey both the superposition principle (3.5),

$$h \circ (f_0 + f_1) = h \circ f_0 + h \circ f_1, \tag{3.16}$$

and the *shift invariance* principle,

$$g(i, j) = f(i + k, j + l) \quad \Leftrightarrow \quad (h \circ g)(i, j) = (h \circ f)(i + k, j + l), \tag{3.17}$$

which means that shifting a signal commutes with applying the operator ($\circ$ stands for the LSI operator). Another way to think of shift invariance is that the operator "behaves the same everywhere".

[4] The continuous version of convolution can be written as $g(\boldsymbol{x}) = \int f(\boldsymbol{x} - \boldsymbol{u})h(\boldsymbol{u})d\boldsymbol{u}$.

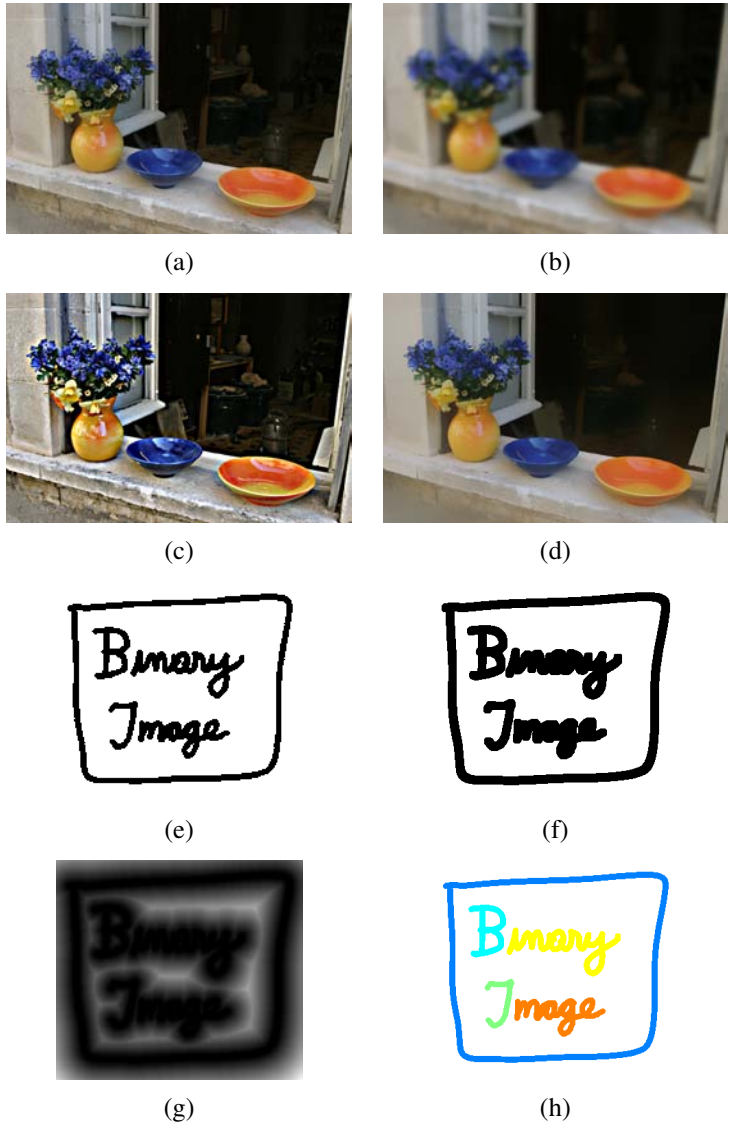

Figure 3.11 Some neighborhood operations: (a) original image; (b) blurred; (c) sharpened; (d) smoothed with edge-preserving filter; (e) binary image; (f) dilated; (g) distance transform; (h) connected components. For the dilation and connected components, black (ink) pixels are assumed to be active, i.e., to have a value of 1 in Equations (3.41–3.45).

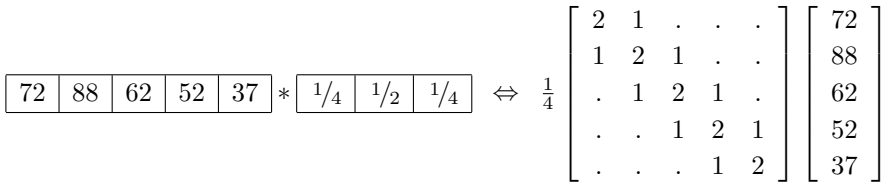

Figure 3.12 One-dimensional signal convolution as a sparse matrix-vector multiply, $\boldsymbol{g} = \boldsymbol{H}\boldsymbol{f}$.

Occasionally, a shift-variant version of correlation or convolution may be used, e.g.,

$$g(i,j) = \sum_{k,l} f(i-k, j-l)h(k,l;i,j), \tag{3.18}$$

where $h(k,l;i,j)$ is the convolution kernel at pixel (i,j). For example, such a spatially varying kernel can be used to model blur in an image due to variable depth-dependent defocus.

Correlation and convolution can both be written as a matrix-vector multiply, if we first convert the two-dimensional images $f(i,j)$ and $g(i,j)$ into raster-ordered vectors $\boldsymbol{f}$ and $\boldsymbol{g}$,

$$\boldsymbol{g} = \boldsymbol{H}\boldsymbol{f}, \tag{3.19}$$

where the (sparse) $\boldsymbol{H}$ matrix contains the convolution kernels. Figure 3.12 shows how a one-dimensional convolution can be represented in matrix-vector form.

Padding (border effects)

The astute reader will notice that the matrix multiply shown in Figure 3.12 suffers from *boundary effects*, i.e., the results of filtering the image in this form will lead to a *darkening* of the corner pixels. This is because the original image is effectively being padded with 0 values wherever the convolution kernel extends beyond the original image boundaries.

To compensate for this, a number of alternative *padding* or extension modes have been developed (Figure 3.13):

- *zero*: set all pixels outside the source image to 0 (a good choice for alpha-matted cutout images);
- *constant (border color)*: set all pixels outside the source image to a specified *border* value;
- *clamp (replicate or clamp to edge)*: repeat edge pixels indefinitely;
- *(cyclic) wrap (repeat or tile)*: loop "around" the image in a "toroidal" configuration;

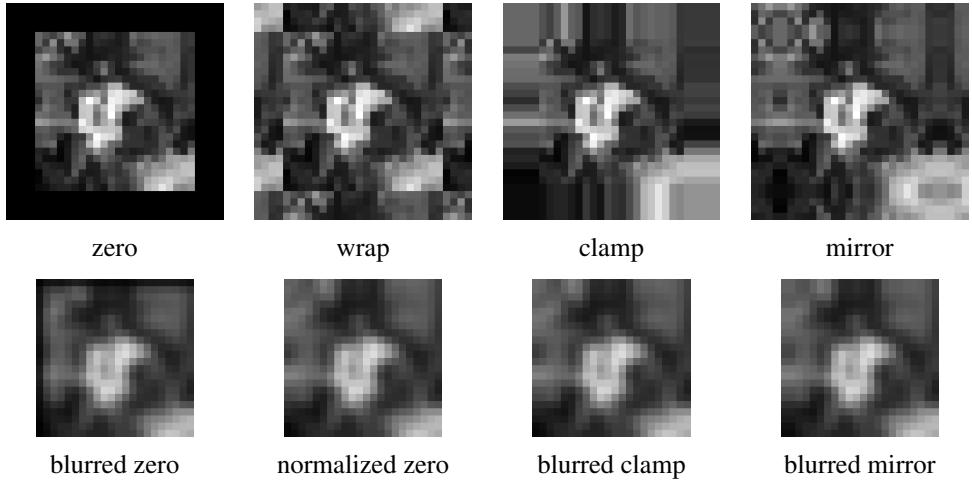

Figure 3.13 Border padding (top row) and the results of blurring the padded image (bottom row). The normalized zero image is the result of dividing (normalizing) the blurred zero-padded RGBA image by its corresponding soft alpha value.

- *mirror*: reflect pixels across the image edge;
- *extend*: extend the signal by subtracting the mirrored version of the signal from the edge pixel value.

In the computer graphics literature (Akenine-Möller and Haines 2002, p. 124), these mechanisms are known as the *wrapping mode* (OpenGL) or *texture addressing mode* (Direct3D). The formulas for each of these modes are left to the reader (Exercise 3.8).

Figure 3.13 shows the effects of padding an image with each of the above mechanisms and then blurring the resulting padded image. As you can see, zero padding darkens the edges, clamp (replication) padding propagates border values inward, mirror (reflection) padding preserves colors near the borders. Extension padding (not shown) keeps the border pixels fixed (during blur).

An alternative to padding is to blur the zero-padded RGBA image and to then divide the resulting image by its alpha value to remove the darkening effect. The results can be quite good, as seen in the normalized zero image in Figure 3.13.

3.2.1 Separable filtering

The process of performing a convolution requires K^2 (multiply-add) operations per pixel, where K is the size (width or height) of the convolution kernel, e.g., the box filter in Fig-

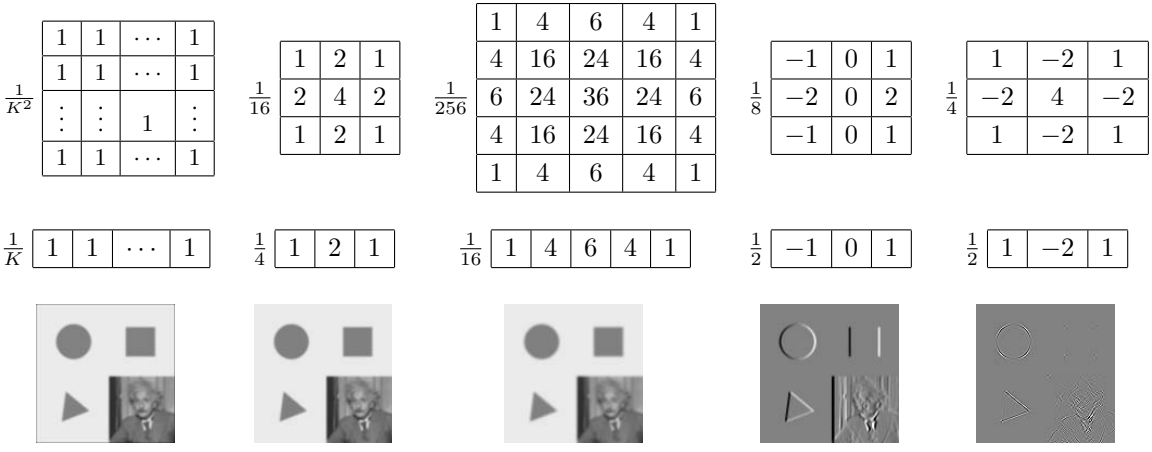

(a) box, $K = 5$ (b) bilinear (c) "Gaussian" (d) Sobel (e) corner

Figure 3.14 Separable linear filters: For each image (a)–(e), we show the 2D filter kernel (top), the corresponding horizontal 1D kernel (middle), and the filtered image (bottom). The filtered Sobel and corner images are signed, scaled up by $2\times$ and $4\times$, respectively, and added to a gray offset before display.

ure 3.14a. In many cases, this operation can be significantly sped up by first performing a one-dimensional horizontal convolution followed by a one-dimensional vertical convolution (which requires a total of $2K$ operations per pixel). A convolution kernel for which this is possible is said to be *separable*.

It is easy to show that the two-dimensional kernel $\boldsymbol{K}$ corresponding to successive convolution with a horizontal kernel $\boldsymbol{h}$ and a vertical kernel $\boldsymbol{v}$ is the *outer product* of the two kernels,

$$\boldsymbol{K} = \boldsymbol{v}\boldsymbol{h}^T \tag{3.20}$$

(see Figure 3.14 for some examples). Because of the increased efficiency, the design of convolution kernels for computer vision applications is often influenced by their separability.

How can we tell if a given kernel $\boldsymbol{K}$ is indeed separable? This can often be done by inspection or by looking at the analytic form of the kernel (Freeman and Adelson 1991). A more direct method is to treat the 2D kernel as a 2D matrix $\boldsymbol{K}$ and to take its singular value decomposition (SVD),

$$\boldsymbol{K} = \sum_i \sigma_i \boldsymbol{u}_i \boldsymbol{v}_i^T \tag{3.21}$$

(see Appendix A.1.1 for the definition of the SVD). If only the first singular value σ_0 is non-zero, the kernel is separable and $\sqrt{\sigma_0}\boldsymbol{u}_0$ and $\sqrt{\sigma_0}\boldsymbol{v}_0^T$ provide the vertical and horizontal

kernels (Perona 1995). For example, the Laplacian of Gaussian kernel (3.26 and 4.23) can be implemented as the sum of two separable filters (4.24) (Wiejak, Buxton, and Buxton 1985).

What if your kernel is not separable and yet you still want a faster way to implement it? Perona (1995), who first made the link between kernel separability and SVD, suggests using more terms in the (3.21) series, i.e., summing up a number of separable convolutions. Whether this is worth doing or not depends on the relative sizes of K and the number of significant singular values, as well as other considerations, such as cache coherency and memory locality.

3.2.2 Examples of linear filtering

Now that we have described the process for performing linear filtering, let us examine a number of frequently used filters.

The simplest filter to implement is the *moving average* or *box* filter, which simply averages the pixel values in a $K \times K$ window. This is equivalent to convolving the image with a kernel of all ones and then scaling (Figure 3.14a). For large kernels, a more efficient implementation is to slide a moving window across each scanline (in a separable filter) while adding the newest pixel and subtracting the oldest pixel from the running sum. This is related to the concept of *summed area tables*, which we describe shortly.

A smoother image can be obtained by separably convolving the image with a piecewise linear "tent" function (also known as a *Bartlett* filter). Figure 3.14b shows a 3×3 version of this filter, which is called the *bilinear* kernel, since it is the outer product of two linear (first-order) splines (see Section 3.5.2).

Convolving the linear tent function with itself yields the cubic approximating spline, which is called the "Gaussian" kernel (Figure 3.14c) in Burt and Adelson's (1983a) *Laplacian pyramid* representation (Section 3.5). Note that approximate Gaussian kernels can also be obtained by iterated convolution with box filters (Wells 1986). In applications where the filters really need to be rotationally symmetric, carefully tuned versions of sampled Gaussians should be used (Freeman and Adelson 1991) (Exercise 3.10).

The kernels we just discussed are all examples of blurring (smoothing) or *low-pass* kernels (since they pass through the lower frequencies while attenuating higher frequencies). How good are they at doing this? In Section 3.4, we use frequency-space Fourier analysis to examine the exact frequency response of these filters. We also introduce the *sinc* ($(\sin x)/x$) filter, which performs *ideal* low-pass filtering.

In practice, smoothing kernels are often used to reduce high-frequency noise. We have much more to say about using variants on smoothing to remove noise later (see Sections 3.3.1, 3.4, and 3.7).

Surprisingly, smoothing kernels can also be used to *sharpen* images using a process called

unsharp masking. Since blurring the image reduces high frequencies, adding some of the difference between the original and the blurred image makes it sharper,

$$g_{\text{sharp}} = f + \gamma(f - h_{\text{blur}} * f). \tag{3.22}$$

In fact, before the advent of digital photography, this was the standard way to sharpen images in the darkroom: create a blurred ("positive") negative from the original negative by misfocusing, then overlay the two negatives before printing the final image, which corresponds to

$$g_{\text{unsharp}} = f(1 - \gamma h_{\text{blur}} * f). \tag{3.23}$$

This is no longer a linear filter but it still works well.

Linear filtering can also be used as a pre-processing stage to edge extraction (Section 4.2) and interest point detection (Section 4.1) algorithms. Figure 3.14d shows a simple 3×3 edge extractor called the Sobel operator, which is a separable combination of a horizontal *central difference* (so called because the horizontal derivative is centered on the pixel) and a vertical tent filter (to smooth the results). As you can see in the image below the kernel, this filter effectively emphasizes horizontal edges.

The simple corner detector (Figure 3.14e) looks for simultaneous horizontal and vertical second derivatives. As you can see however, it responds not only to the corners of the square, but also along diagonal edges. Better corner detectors, or at least interest point detectors that are more rotationally invariant, are described in Section 4.1.

3.2.3 Band-pass and steerable filters

The Sobel and corner operators are simple examples of band-pass and oriented filters. More sophisticated kernels can be created by first smoothing the image with a (unit area) Gaussian filter,

$$G(x, y; \sigma) = \frac{1}{2\pi\sigma^2} e^{-\frac{x^2+y^2}{2\sigma^2}}, \tag{3.24}$$

and then taking the first or second derivatives (Marr 1982; Witkin 1983; Freeman and Adelson 1991). Such filters are known collectively as *band-pass filters*, since they filter out both low and high frequencies.

The (undirected) second derivative of a two-dimensional image,

$$\nabla^2 f = \frac{\partial^2 f}{\partial x^2} + \frac{\partial^2 y}{\partial y^2}, \tag{3.25}$$

is known as the *Laplacian* operator. Blurring an image with a Gaussian and then taking its Laplacian is equivalent to convolving directly with the *Laplacian of Gaussian* (LoG) filter,

$$\nabla^2 G(x, y; \sigma) = \left(\frac{x^2 + y^2}{\sigma^4} - \frac{2}{\sigma^2} \right) G(x, y; \sigma), \tag{3.26}$$

(a) (b) (c)

Figure 3.15 Second-order steerable filter (Freeman 1992) © 1992 IEEE: (a) original image of Einstein; (b) orientation map computed from the second-order oriented energy; (c) original image with oriented structures enhanced.

which has certain nice *scale-space properties* (Witkin 1983; Witkin, Terzopoulos, and Kass 1986). The five-point Laplacian is just a compact approximation to this more sophisticated filter.

Likewise, the Sobel operator is a simple approximation to a *directional* or *oriented* filter, which can obtained by smoothing with a Gaussian (or some other filter) and then taking a *directional derivative* $\nabla_{\hat{\boldsymbol{u}}} = \frac{\partial}{\partial \hat{\boldsymbol{u}}}$, which is obtained by taking the dot product between the gradient field ∇ and a unit direction $\hat{\boldsymbol{u}} = (\cos\theta, \sin\theta)$,

$$\hat{\boldsymbol{u}} \cdot \nabla(G * f) = \nabla_{\hat{\boldsymbol{u}}}(G * f) = (\nabla_{\hat{\boldsymbol{u}}} G) * f. \tag{3.27}$$

The smoothed directional derivative filter,

$$G_{\hat{\boldsymbol{u}}} = uG_x + vG_y = u\frac{\partial G}{\partial x} + v\frac{\partial G}{\partial y}, \tag{3.28}$$

where $\hat{\boldsymbol{u}} = (u, v)$, is an example of a *steerable* filter, since the value of an image convolved with $G_{\hat{\boldsymbol{u}}}$ can be computed by first convolving with the pair of filters (G_x, G_y) and then *steering* the filter (potentially locally) by multiplying this gradient field with a unit vector $\hat{\boldsymbol{u}}$ (Freeman and Adelson 1991). The advantage of this approach is that a whole *family* of filters can be evaluated with very little cost.

How about steering a directional second derivative filter $\nabla_{\hat{\boldsymbol{u}}} \cdot \nabla_{\hat{\boldsymbol{u}}} G_{\hat{\boldsymbol{u}}}$, which is the result of taking a (smoothed) directional derivative and then taking the directional derivative again? For example, G_{xx} is the second directional derivative in the x direction.

At first glance, it would appear that the steering trick will not work, since for every direction $\hat{\boldsymbol{u}}$, we need to compute a different first directional derivative. Somewhat surprisingly, Freeman and Adelson (1991) showed that, for directional Gaussian derivatives, it is possible

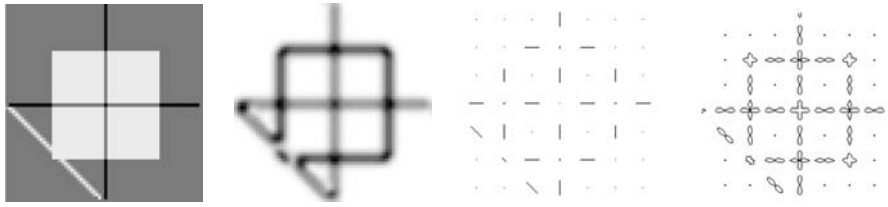

(a) (b) (c) (d)

Figure 3.16 Fourth-order steerable filter (Freeman and Adelson 1991) © 1991 IEEE: (a) test image containing bars (lines) and step edges at different orientations; (b) average oriented energy; (c) dominant orientation; (d) oriented energy as a function of angle (polar plot).

to steer *any* order of derivative with a relatively small number of basis functions. For example, only three basis functions are required for the second-order directional derivative,

$$G_{\hat{\boldsymbol{u}}\hat{\boldsymbol{u}}} = u^2 G_{xx} + 2uv G_{xy} + v^2 G_{yy}. \tag{3.29}$$

Furthermore, each of the basis filters, while not itself necessarily separable, can be computed using a linear combination of a small number of separable filters (Freeman and Adelson 1991).

This remarkable result makes it possible to construct directional derivative filters of increasingly greater *directional selectivity*, i.e., filters that only respond to edges that have strong local consistency in orientation (Figure 3.15). Furthermore, higher order steerable filters can respond to potentially more than a single edge orientation at a given location, and they can respond to both *bar* edges (thin lines) and the classic step edges (Figure 3.16). In order to do this, however, full *Hilbert transform pairs* need to be used for second-order and higher filters, as described in (Freeman and Adelson 1991).

Steerable filters are often used to construct both feature descriptors (Section 4.1.3) and edge detectors (Section 4.2). While the filters developed by Freeman and Adelson (1991) are best suited for detecting linear (edge-like) structures, more recent work by Koethe (2003) shows how a combined 2×2 boundary tensor can be used to encode both edge and junction ("corner") features. Exercise 3.12 has you implement such steerable filters and apply them to finding both edge and corner features.

Summed area table (integral image)

If an image is going to be repeatedly convolved with different box filters (and especially filters of different sizes at different locations), you can precompute the *summed area table* (Crow

3	2	7	2	3
1	5	1	3	4
5	1	**3**	5	1
4	3	2	1	6
2	4	1	4	8

(a) S = 24

3	5	12	14	17
4	*11*	**19**	24	31
9	**17**	28	38	46
13	24	37	48	62
15	30	44	59	81

(b) s = 28

3	5	12	*14*	17
4	11	19	24	31
9	17	28	38	46
13	24	37	**48**	62
15	30	44	59	81

(c) S = 24

Figure 3.17 Summed area tables: (a) original image; (b) summed area table; (c) computation of area sum. Each value in the summed area table $s(i, j)$ (red) is computed recursively from its three adjacent (blue) neighbors (3.31). Area sums S (green) are computed by combining the four values at the rectangle corners (purple) (3.32). Positive values are shown in **bold** and negative values in *italics*.

1984), which is just the running sum of all the pixel values from the origin,

$$s(i, j) = \sum_{k=0}^{i} \sum_{l=0}^{j} f(k, l). \tag{3.30}$$

This can be efficiently computed using a recursive (raster-scan) algorithm,

$$s(i, j) = s(i - 1, j) + s(i, j - 1) - s(i - 1, j - 1) + f(i, j). \tag{3.31}$$

The image $s(i, j)$ is also often called an *integral image* (see Figure 3.17) and can actually be computed using only two additions per pixel if separate row sums are used (Viola and Jones 2004). To find the summed area (integral) inside a rectangle $[i_0, i_1] \times [j_0, j_1]$, we simply combine four samples from the summed area table,

$$S(i_0 \ldots i_1, j_0 \ldots j_1) = \sum_{i=i_0}^{i_1} \sum_{j=j_0}^{j_1} s(i_1, j_1) - s(i_1, j_0 - 1) - s(i_0 - 1, j_1) + s(i_0 - 1, j_0 - 1). \tag{3.32}$$

A potential disadvantage of summed area tables is that they require $\log M + \log N$ extra bits in the accumulation image compared to the original image, where M and N are the image width and height. Extensions of summed area tables can also be used to approximate other convolution kernels (Wolberg (1990, Section 6.5.2) contains a review).

In computer vision, summed area tables have been used in face detection (Viola and Jones 2004) to compute simple multi-scale low-level features. Such features, which consist of adjacent rectangles of positive and negative values, are also known as *boxlets* (Simard, Bottou,

Haffner *et al.* 1998). In principle, summed area tables could also be used to compute the sums in the sum of squared differences (SSD) stereo and motion algorithms (Section 11.4). In practice, separable moving average filters are usually preferred (Kanade, Yoshida, Oda *et al.* 1996), unless many different window shapes and sizes are being considered (Veksler 2003).

Recursive filtering

The incremental formula (3.31) for the summed area is an example of a *recursive filter*, i.e., one whose values depends on previous filter outputs. In the signal processing literature, such filters are known as *infinite impulse response* (IIR), since the output of the filter to an impulse (single non-zero value) goes on forever. For example, for a summed area table, an impulse generates an infinite rectangle of 1s below and to the right of the impulse. The filters we have previously studied in this chapter, which involve the image with a finite extent kernel, are known as *finite impulse response* (FIR).

Two-dimensional IIR filters and recursive formulas are sometimes used to compute quantities that involve large area interactions, such as two-dimensional distance functions (Section 3.3.3) and connected components (Section 3.3.4).

More commonly, however, IIR filters are used inside one-dimensional separable filtering stages to compute large-extent smoothing kernels, such as efficient approximations to Gaussians and edge filters (Deriche 1990; Nielsen, Florack, and Deriche 1997). Pyramid-based algorithms (Section 3.5) can also be used to perform such large-area smoothing computations.

3.3 More neighborhood operators

As we have just seen, linear filters can perform a wide variety of image transformations. However non-linear filters, such as edge-preserving median or bilateral filters, can sometimes perform even better. Other examples of neighborhood operators include *morphological* operators that operate on binary images, as well as *semi-global* operators that compute *distance transforms* and find *connected components* in binary images (Figure 3.11f–h).

3.3.1 Non-linear filtering

The filters we have looked at so far have all been *linear*, i.e., their response to a sum of two signals is the same as the sum of the individual responses. This is equivalent to saying that each output pixel is a weighted summation of some number of input pixels (3.19). Linear filters are easier to compose and are amenable to frequency response analysis (Section 3.4).

In many cases, however, better performance can be obtained by using a *non-linear* combination of neighboring pixels. Consider for example the image in Figure 3.18e, where the

Chapter 6

Feature-based alignment

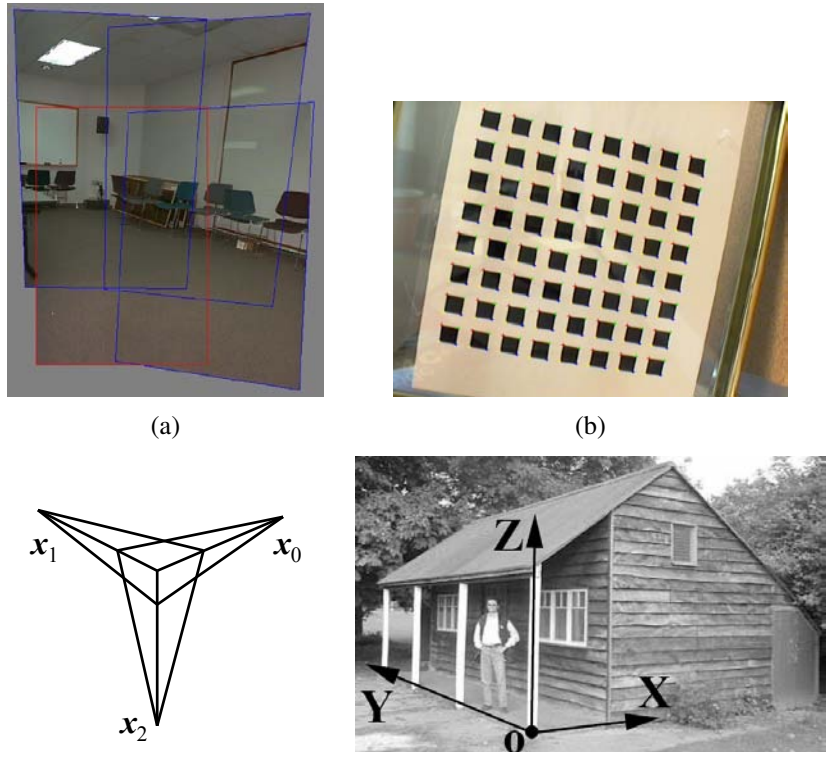

Figure 6.1 Geometric alignment and calibration: (a) geometric alignment of 2D images for stitching (Szeliski and Shum 1997) © 1997 ACM; (b) a two-dimensional calibration target (Zhang 2000) © 2000 IEEE; (c) calibration from vanishing points; (d) scene with easy-to-find lines and vanishing directions (Criminisi, Reid, and Zisserman 2000) © 2000 Springer.

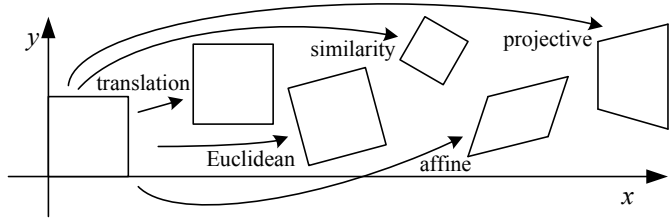

Figure 6.2 Basic set of 2D planar transformations

Once we have extracted features from images, the next stage in many vision algorithms is to match these features across different images (Section 4.1.3). An important component of this matching is to verify whether the set of matching features is geometrically consistent, e.g., whether the feature displacements can be described by a simple 2D or 3D geometric transformation. The computed motions can then be used in other applications such as image stitching (Chapter 9) or augmented reality (Section 6.2.3).

In this chapter, we look at the topic of geometric image registration, i.e., the computation of 2D and 3D transformations that map features in one image to another (Section 6.1). One special case of this problem is *pose estimation*, which is determining a camera's position relative to a known 3D object or scene (Section 6.2). Another case is the computation of a camera's *intrinsic calibration*, which consists of the internal parameters such as focal length and radial distortion (Section 6.3). In Chapter 7, we look at the related problems of how to estimate 3D point structure from 2D matches (*triangulation*) and how to simultaneously estimate 3D geometry and camera motion (*structure from motion*).

6.1 2D and 3D feature-based alignment

Feature-based alignment is the problem of estimating the motion between two or more sets of matched 2D or 3D points. In this section, we restrict ourselves to global *parametric* transformations, such as those described in Section 2.1.2 and shown in Table 2.1 and Figure 6.2, or higher order transformation for curved surfaces (Shashua and Toelg 1997; Can, Stewart, Roysam *et al.* 2002). Applications to non-rigid or elastic deformations (Bookstein 1989; Szeliski and Lavallée 1996; Torresani, Hertzmann, and Bregler 2008) are examined in Sections 8.3 and 12.6.4.

Transform	Matrix	Parameters $\boldsymbol{p}$	Jacobian $\boldsymbol{J}$
translation	$\begin{bmatrix} 1 & 0 & t_x \\ 0 & 1 & t_y \end{bmatrix}$	(t_x, t_y)	$\begin{bmatrix} 1 & 0 \\ 0 & 1 \end{bmatrix}$
Euclidean	$\begin{bmatrix} c_\theta & -s_\theta & t_x \\ s_\theta & c_\theta & t_y \end{bmatrix}$	(t_x, t_y, θ)	$\begin{bmatrix} 1 & 0 & -s_\theta x - c_\theta y \\ 0 & 1 & c_\theta x - s_\theta y \end{bmatrix}$
similarity	$\begin{bmatrix} 1+a & -b & t_x \\ b & 1+a & t_y \end{bmatrix}$	(t_x, t_y, a, b)	$\begin{bmatrix} 1 & 0 & x & -y \\ 0 & 1 & y & x \end{bmatrix}$
affine	$\begin{bmatrix} 1+a_{00} & a_{01} & t_x \\ a_{10} & 1+a_{11} & t_y \end{bmatrix}$	$(t_x, t_y, a_{00}, a_{01}, a_{10}, a_{11})$	$\begin{bmatrix} 1 & 0 & x & y & 0 & 0 \\ 0 & 1 & 0 & 0 & x & y \end{bmatrix}$
projective	$\begin{bmatrix} 1+h_{00} & h_{01} & h_{02} \\ h_{10} & 1+h_{11} & h_{12} \\ h_{20} & h_{21} & 1 \end{bmatrix}$	$(h_{00}, h_{01}, \ldots, h_{21})$	(see Section 6.1.3)

Table 6.1 Jacobians of the 2D coordinate transformations $\boldsymbol{x}' = \boldsymbol{f}(\boldsymbol{x}; \boldsymbol{p})$ shown in Table 2.1, where we have re-parameterized the motions so that they are identity for $\boldsymbol{p} = 0$.

6.1.1 2D alignment using least squares

Given a set of matched feature points $\{(\boldsymbol{x}_i, \boldsymbol{x}'_i)\}$ and a planar parametric transformation[1] of the form

$$\boldsymbol{x}' = \boldsymbol{f}(\boldsymbol{x}; \boldsymbol{p}), \tag{6.1}$$

how can we produce the best estimate of the motion parameters $\boldsymbol{p}$? The usual way to do this is to use least squares, i.e., to minimize the sum of squared residuals

$$E_{\mathrm{LS}} = \sum_i \|\boldsymbol{r}_i\|^2 = \sum_i \|\boldsymbol{f}(\boldsymbol{x}_i; \boldsymbol{p}) - \boldsymbol{x}'_i\|^2, \tag{6.2}$$

where

$$\boldsymbol{r}_i = \boldsymbol{f}(\boldsymbol{x}_i; \boldsymbol{p}) - \boldsymbol{x}'_i = \hat{\boldsymbol{x}}'_i - \tilde{\boldsymbol{x}}'_i \tag{6.3}$$

is the *residual* between the measured location $\hat{\boldsymbol{x}}'_i$ and its corresponding current *predicted* location $\tilde{\boldsymbol{x}}'_i = \boldsymbol{f}(\boldsymbol{x}_i; \boldsymbol{p})$. (See Appendix A.2 for more on least squares and Appendix B.2 for a statistical justification.)

[1] For examples of non-planar parametric models, such as quadrics, see the work of Shashua and Toelg (1997); Shashua and Wexler (2001).

Many of the motion models presented in Section 2.1.2 and Table 2.1, i.e., translation, similarity, and affine, have a *linear* relationship between the amount of motion $\Delta \boldsymbol{x} = \boldsymbol{x}' - \boldsymbol{x}$ and the unknown parameters $\boldsymbol{p}$,

$$\Delta \boldsymbol{x} = \boldsymbol{x}' - \boldsymbol{x} = \boldsymbol{J}(\boldsymbol{x})\boldsymbol{p}, \tag{6.4}$$

where $\boldsymbol{J} = \partial \boldsymbol{f}/\partial \boldsymbol{p}$ is the *Jacobian* of the transformation $\boldsymbol{f}$ with respect to the motion parameters $\boldsymbol{p}$ (see Table 6.1). In this case, a simple *linear* regression (linear least squares problem) can be formulated as

$$\begin{aligned} E_{\mathrm{LLS}} &= \sum_i \|\boldsymbol{J}(\boldsymbol{x}_i)\boldsymbol{p} - \Delta \boldsymbol{x}_i\|^2 && (6.5) \\ &= \boldsymbol{p}^T \left[\sum_i \boldsymbol{J}^T(\boldsymbol{x}_i)\boldsymbol{J}(\boldsymbol{x}_i)\right] \boldsymbol{p} - 2\boldsymbol{p}^T \left[\sum_i \boldsymbol{J}^T(\boldsymbol{x}_i)\Delta \boldsymbol{x}_i\right] + \sum_i \|\Delta \boldsymbol{x}_i\|^2 && (6.6) \\ &= \boldsymbol{p}^T \boldsymbol{A}\boldsymbol{p} - 2\boldsymbol{p}^T \boldsymbol{b} + c. && (6.7) \end{aligned}$$

The minimum can be found by solving the symmetric positive definite (SPD) system of *normal equations*[2]

$$\boldsymbol{A}\boldsymbol{p} = \boldsymbol{b}, \tag{6.8}$$

where

$$\boldsymbol{A} = \sum_i \boldsymbol{J}^T(\boldsymbol{x}_i)\boldsymbol{J}(\boldsymbol{x}_i) \tag{6.9}$$

is called the *Hessian* and $\boldsymbol{b} = \sum_i \boldsymbol{J}^T(\boldsymbol{x}_i)\Delta \boldsymbol{x}_i$. For the case of pure translation, the resulting equations have a particularly simple form, i.e., the translation is the average translation between corresponding points or, equivalently, the translation of the point centroids.

Uncertainty weighting. The above least squares formulation assumes that all feature points are matched with the same accuracy. This is often not the case, since certain points may fall into more textured regions than others. If we associate a scalar variance estimate σ_i^2 with each correspondence, we can minimize the *weighted least squares* problem instead,[3]

$$E_{\mathrm{WLS}} = \sum_i \sigma_i^{-2} \|\boldsymbol{r}_i\|^2. \tag{6.10}$$

As shown in Section 8.1.3, a covariance estimate for patch-based matching can be obtained by multiplying the inverse of the *patch Hessian* $\boldsymbol{A}_i$ (8.55) with the per-pixel noise covariance

[2] For poorly conditioned problems, it is better to use QR decomposition on the set of linear equations $\boldsymbol{J}(\boldsymbol{x}_i)\boldsymbol{p} = \Delta \boldsymbol{x}_i$ instead of the normal equations (Björck 1996; Golub and Van Loan 1996). However, such conditions rarely arise in image registration.

[3] Problems where each measurement can have a different variance or certainty are called *heteroscedastic models*.

Figure 6.3 A simple panograph consisting of three images automatically aligned with a translational model and then averaged together.

σ_n^2 (8.44). Weighting each squared residual by its inverse covariance $\Sigma_i^{-1} = \sigma_n^{-2}\boldsymbol{A}_i$ (which is called the *information matrix*), we obtain

$$E_{\mathrm{CWLS}} = \sum_i \|\boldsymbol{r}_i\|^2_{\Sigma_i^{-1}} = \sum_i \boldsymbol{r}_i^T \Sigma_i^{-1} \boldsymbol{r}_i = \sum_i \sigma_n^{-2} \boldsymbol{r}_i^T \boldsymbol{A}_i \boldsymbol{r}_i. \tag{6.11}$$

6.1.2 *Application*: Panography

One of the simplest (and most fun) applications of image alignment is a special form of image stitching called *panography*. In a panograph, images are translated and optionally rotated and scaled before being blended with simple averaging (Figure 6.3). This process mimics the photographic collages created by artist David Hockney, although his compositions use an opaque overlay model, being created out of regular photographs.

In most of the examples seen on the Web, the images are aligned by hand for best artistic effect.[4] However, it is also possible to use feature matching and alignment techniques to perform the registration automatically (Nomura, Zhang, and Nayar 2007; Zelnik-Manor and Perona 2007).

Consider a simple translational model. We want all the corresponding features in different images to line up as best as possible. Let $\boldsymbol{t}_j$ be the location of the jth image coordinate frame in the global composite frame and $\boldsymbol{x}_{ij}$ be the location of the ith matched feature in the jth image. In order to align the images, we wish to minimize the least squares error

$$E_{\mathrm{PLS}} = \sum_{ij} \|(\boldsymbol{t}_j + \boldsymbol{x}_{ij}) - \boldsymbol{x}_i\|^2, \tag{6.12}$$

[4] http://www.flickr.com/groups/panography/.

where $\boldsymbol{x}_i$ is the consensus (average) position of feature i in the global coordinate frame. (An alternative approach is to register each pair of overlapping images separately and then compute a consensus location for each frame—see Exercise 6.2.)

The above least squares problem is indeterminate (you can add a constant offset to all the frame and point locations $\boldsymbol{t}_j$ and $\boldsymbol{x}_i$). To fix this, either pick one frame as being at the origin or add a constraint to make the average frame offsets be 0.

The formulas for adding rotation and scale transformations are straightforward and are left as an exercise (Exercise 6.2). See if you can create some collages that you would be happy to share with others on the Web.

6.1.3 Iterative algorithms

While linear least squares is the simplest method for estimating parameters, most problems in computer vision do not have a simple linear relationship between the measurements and the unknowns. In this case, the resulting problem is called *non-linear least squares* or *non-linear regression*.

Consider, for example, the problem of estimating a rigid Euclidean 2D transformation (translation plus rotation) between two sets of points. If we parameterize this transformation by the translation amount (t_x, t_y) and the rotation angle θ, as in Table 2.1, the Jacobian of this transformation, given in Table 6.1, depends on the current value of θ. Notice how in Table 6.1, we have re-parameterized the motion matrices so that they are always the identity at the origin $\boldsymbol{p} = 0$, which makes it easier to initialize the motion parameters.

To minimize the non-linear least squares problem, we iteratively find an update $\Delta\boldsymbol{p}$ to the current parameter estimate $\boldsymbol{p}$ by minimizing

$$
\begin{aligned}
E_{\mathrm{NLS}}(\Delta\boldsymbol{p}) &= \sum_i \|\boldsymbol{f}(\boldsymbol{x}_i;\boldsymbol{p}+\Delta\boldsymbol{p}) - \boldsymbol{x}_i'\|^2 && (6.13)\\
&\approx \sum_i \|\boldsymbol{J}(\boldsymbol{x}_i;\boldsymbol{p})\Delta\boldsymbol{p} - \boldsymbol{r}_i\|^2 && (6.14)\\
&= \Delta\boldsymbol{p}^T\left[\sum_i \boldsymbol{J}^T\boldsymbol{J}\right]\Delta\boldsymbol{p} - 2\Delta\boldsymbol{p}^T\left[\sum_i \boldsymbol{J}^T\boldsymbol{r}_i\right] + \sum_i \|\boldsymbol{r}_i\|^2 && (6.15)\\
&= \Delta\boldsymbol{p}^T\boldsymbol{A}\Delta\boldsymbol{p} - 2\Delta\boldsymbol{p}^T\boldsymbol{b} + c, && (6.16)
\end{aligned}
$$

where the "Hessian"[5] $\boldsymbol{A}$ is the same as Equation (6.9) and the right hand side vector

$$\boldsymbol{b} = \sum_i \boldsymbol{J}^T(\boldsymbol{x}_i)\boldsymbol{r}_i \qquad (6.17)$$

[5] The "Hessian" $\boldsymbol{A}$ is not the true Hessian (second derivative) of the non-linear least squares problem (6.13). Instead, it is the approximate Hessian, which neglects second (and higher) order derivatives of $\boldsymbol{f}(\boldsymbol{x}_i;\boldsymbol{p}+\Delta\boldsymbol{p})$.